UI-MoCap: An Integrated UWB-IMU Circuit Enables 3D Positioning and Enhances IMU Data Transmission

Wenjuan Zhong, Lei Zhang, Zhongbo Sun, Mingjie Dong, *Senior Member, IEEE*, and Mingming Zhang, *Senior Member, IEEE*

***Abstract*— While inertial measurement unit (IMU)-based motion capture (MoCap) systems have been gaining popularity for human movement analysis, they still suffer from long-term positioning errors due to accumulated drift and inefficient data transmission via Wi-Fi or Bluetooth. To address this problem, this study introduces an integrated ultrawideband (UWB)-IMU system, named UI-MoCap, designed for simultaneous 3D positioning as well as wireless IMU data transmission through UWB pulses. The UI-MoCap comprises mobile UWB tags and hardware-synchronized UWB base stations. Each UWB tag, a compact circular PCB with a 3.4cm diameter, houses a nine-axis IMU unit and a UWB transceiver for data transmission. The base stations are equipped with a UWB transceiver and an Ethernet controller, ensuring efficient reception and management of messages from multiple tags. Experiments were conducted to evaluate the system's validity and reliability of 3D positioning and IMU data transmission. The results demonstrate that UI-MoCap achieves centimeter-level 3D positioning accuracy and maintains consistent positioning performance over time. Moreover, UI-MoCap exhibits high update rates and a minimal packet loss rate for IMU data transmission, significantly outperforming Wi-Fi-based transmission techniques. Future work will explore the fusion of UWB and IMU technologies to further enhance positioning performance, with a focus on human movement analysis and rehabilitation applications.**

Manuscript received 7 November 2023; revised 28 January 2024; accepted 20 February 2024. Date of publication 26 February 2024; date of current version 1 March 2024. This work was supported in part by the National Key Research and Development Program of China under Grant 2023YFF1205200, in part by Shenzhen Science and Technology Program under Grant JCYJ20220530113811027 and Grant JCYJ20210324104203010, and in part by Guangdong Provincial Key Laboratory of Advanced Biomaterials under Grant 2022B1212010003. *(Wenjuan Zhong and Lei Zhang contributed equally to this work.) (Corresponding authors: Mingjie Dong; Mingming Zhang.)*

Wenjuan Zhong, Lei Zhang, and Mingming Zhang are with Shenzhen Key Laboratory of Smart Healthcare Engineering, Department of Biomedical Engineering, College of Engineering, Southern University of Science and Technology, Shenzhen 518055, China (e-mail: zhongwj@mail.sustech.edu.cn; 12232561@mail.sustech.edu.cn; zhangmm@sustech.edu.cn).

Zhongbo Sun is with the Department of Control Engineering, Changchun University of Technology, Changchun 130012, China (e-mail: zbsun@ccut.edu.cn).

Mingjie Dong is with Beijing Key Laboratory of Advanced Manufacturing Technology, Faculty of Materials and Manufacturing, Beijing University of Technology, Beijing 100124, China (e-mail: dongmj@bjut.edu.cn).

This article has supplementary downloadable material available at https://doi.org/10.1109/TNSRE.2024.3369647, provided by the authors.

Digital Object Identifier 10.1109/TNSRE.2024.3369647

***Index Terms*— Motion capture technology, inertial measurement unit (IMU), ultrawideband (UWB), position detection.**

I. Introduction

MOTION capture (MoCap) is designed for continuous monitoring, tracking, and recording of human body movements in three-dimensional (3D) space [1], [2]. This technology plays an important role in diverse domains, notably in sports training [3], film industry [4], human-robot interaction [5], [6], and rehabilitation training [7], [8]. Optoelectronic MoCap systems are typically accepted as the gold standard because they can achieve precise 3D motion tracking by measuring the infrared line reflected from markers [2], [9]. However, they come with the trade-offs of complex setup requirements, labor-intensive post-processing, and high cost [9]. In contrast, inertial measurement units (IMUs)-based MoCap systems show greater potential in portability and economy.

IMUs have been developed to effectively record human limb segment movements [10], [11]. While wearable IMUs excel in providing orientation information vital for motion capture, they inherently fall short in furnishing absolute body position data. Typically, numeric integration techniques are applied to the outputs from IMUs to achieve motion positioning. However, this approach is susceptible to the cumulative drift effect over time [12]. To cope with this issue, researchers have proposed certain strategies to minimize drift-related errors. For instance, Foxlin et al. introduced the zero velocity updates (ZUPTs) method that minimizes position errors by assuming zero velocity during non-movement intervals [13]; Yuan et al. incorporated force sensors to detect locomotion phases and further determine the spatial position of a reference point on the human body [14]. Although these methods significantly enhance the performance of inertial-based motion positioning, the drift-related errors are not completely eliminated and continue to accumulate over time.

Ultrawideband (UWB) technology, being a radio-frequency-based system, can consistently provide accurate and drift-free positioning data over time [15], [16], [17]. UWB, which utilizes nanosecond non-sinusoidal narrow pulse signals for transmitting data, has been widely recognized as an effective technology within location-aware sensor networks [18], [19].

© 2024 The Authors. This work is licensed under a Creative Commons Attribution 4.0 License.
For more information, see https://creativecommons.org/licenses/by/4.0/

Its appeal lies not only in delivering centimeter-level precision at an affordable cost but also in exhibiting robustness against multipath effects [19], [20]. However, it is imperative to note that UWB operates within a high-frequency band, making it most effective in line-of-sight (LOS) conditions. In the presence of metal obstacles, its positioning accuracy is significantly reduced, posing challenges in complex indoor environments [19]. Hence, relying solely on UWB may hinder the attainment of high-precision positioning.

To achieve both accuracy and robustness in MoCap systems, researchers have explored synergistic potential of sensor fusion algorithms, integrating data from UWB tags and IMU sensors [21], [22], [23]. Zhong et al. proposed an integrated IMU-UWB algorithm for reliable and continuous indoor positioning in X-Y horizontal plane, particularly in non-line-of-sight (NLOS) conditions [21]. In addition, some studies have combined IMU-UWB fusion algorithms with human biomechanical models to implement 3D trajectory tracking of human lower limbs [22], [23], [24]. For instance, Zihajehzadeh et al. applied a sensor fusion algorithm to a lower-body biomechanical model, demonstrating its capability to enhance the accuracy of 3D body location and knee joint angle tracking [22]. However, in previous works [21], [22], [23], [24], IMU and UWB were treated as two independent hardware modules, in which IMU data were transmitted through Wi-Fi or Bluetooth rather than UWB, and UWB functioned solely for absolute positioning. Such non-integrated hardware configuration increases the system complexity. Additionally, the transmission of IMU signals through Wi-Fi or Bluetooth restricts their effectiveness in indoor environments due to signal interference [19].

Another crucial aspect often overlooked in integrated UWB-IMU Mocap system is the capability for multi-tag support. Existing IMU/UWB fusion systems typically accommodate only a limited number of UWB tags due to the challenges associated with (i) managing the transmission of a large volume of messages and (ii) implementing scheduling techniques to avoid collision [25]. For example, in existing lower-limb MoCap systems relying on IMU/UWB fusion architecture, it is common practice to support only one or three UWB tags affixed to human waists or feet as the root position reference [22], [23], [24]. The absolute positions of human hip, knee, and ankle joints are determined through forward kinematic calculations based on root position reference and joint angles derived from the numeric integration of IMU outputs [22]. Such approach can introduce accumulative errors into the estimated joint angles, further worsen positioning accuracy.

Aiming to address the aforementioned challenges, this study introduces an integrated UWB-IMU circuit, named UI-MoCap, that enables multi-tag 3D positioning and wireless IMU data transmission via UWB. The core of this positioning system comprises UWB mobile tags, each of which is equipped with replaceable IMU modules, enabling IMU signals transmission via UWB nanosecond pulses. These pulses are received by the second component of the system, which consists of several hardware-synchronized UWB base stations. The base stations employ time division multiple access (TDMA) techniques to effectively manage IMU data from multiple tags. The system performance was preliminarily evaluated from two aspects: 1) the validity and reliability on 3D positioning accuracy in both stationary and dynamic scenarios, and 2) capability of wireless multiple IMU data transmission in comparison to Wi-Fi. The primary contributions of this article can be outlined as follows:

1) An integrated UWB-IMU hardware system, named UI-MoCap, is proposed, which seamlessly integrates nine-axis IMU modules into multiple UWB mobile tags. UI-MoCap can precisely collect timestamps to facilitate accurate tag position computation using the time difference of arrival (TDoA) method, and effectively manage IMU data transmission from multiple tags.
2) Evaluation results demonstrate the system's exceptional capability in achieving centimeter-level positioning accuracy, with a positioning error of 1.86cm in static experiments and 3.20cm in dynamic tests. Furthermore, with a high update rate of 100Hz, UI-MoCap exhibits significantly lower packet loss rates for multiple IMU data transmission compared to Wi-Fi-based techniques.

II. Related Works

This section will introduce principles underlying four types of UWB-based positioning methods: two-way ranging (TWR), TDoA, angle of arrival (AoA), and concurrent technique. Additionally, we will detail on the advantages and disadvantages of each approach, considering their suitability for both positioning and message transmission in MoCap applications.

A. TWR

TWR determines the tag's position by measuring the distance between each base station and the tag as Fig. 1(a) shows. In the TWR deployment, multiple messages are transferred between the tag and base station to locate the tag. Fig. 2(a) represents the time scheme of TWR, which is proposed by Neirynck et al. [26], where $BS1$, $BS2$ refer to different base stations. We will use the following notations: $B \in \{b_1, b_2, \cdots, b_N\}$ refers to different base stations, t refers to the tag. $S \in \{t, b_1, b_2, \cdots, b_n\}$ refers to all the subjects. $T_{S,N}$ refers to time measured by S. D_{S_1,S_2} refers the distance between subject S_1 and S_2. $X_S = (x_S, y_S, z_S)$ means the coordinate of S. Suppose we have already known the coordinates of base stations X_B, the measured distance $\hat{D}_{b_1,t}$ between base station b_1 and tag t can be calculated as:

$$\hat{D}_{b_1,t} = \frac{c}{4}\left[\begin{array}{l}\left(T_{b_1,3} - T_{b_1,2}\right) - \left(T_{b_1,2} - T_{b_1,1}\right) \\ + \left(T_{t,2} - T_{t,1}\right) - \left(T_{t,4} - T_{t,2}\right)\end{array}\right] \tag{1}$$

where c refer to the speed of light. After attaining all the distance, we can solve the position X_t by:

$$X_t = \underset{X_t}{\operatorname{argmin}} \sum_{i=1}^{N} \left(D_{b_i,t} - \hat{D}_{b_i,t}\right)^2 \tag{2}$$

where:

$$D_{b_i,t} = \|X_t - X_{b_i}\| \tag{3}$$

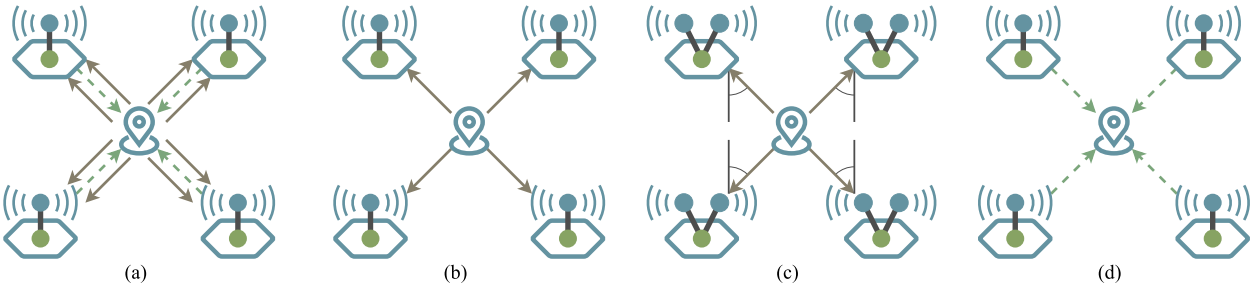

Fig. 1. UWB positioning techniques. (a) Two-way ranging (TWR). (b) Time difference of arrival (TDoA). (c) Angle of arrival (AoA). (d) Concurrent technique.

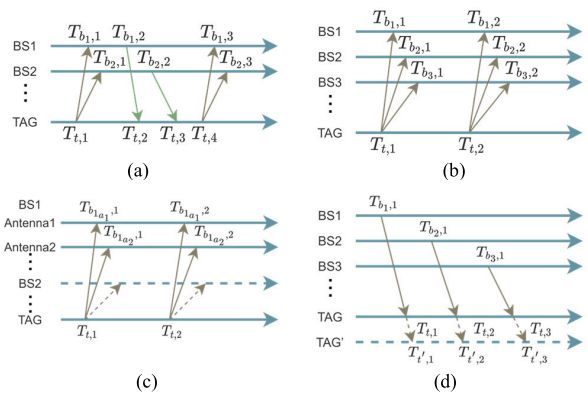

Fig. 2. Time scheme of UWB positioning techniques. (a) Two-way ranging (TWR). (b) Time difference of arrival (TDoA). (c) Angle of arrival (AoA). (d) Concurrent technique.

One major benefit of the TWR-based system is that it eliminates the requirement for synchronizing base stations while maintaining high location accuracy, which makes it convenient to deploy. Because of this advantage, TWR-based systems are widely used in different scenarios, such as underground mines [27], merchant vessels [28], and personal devices [29]. However, they have certain disadvantages. The bidirectional communication between tags and base stations increases the complexity of positioning. These methods also require the exchange of large number messages, resulting in low update rates of message transmission.

B. TDoA

TDoA calculates the tag's position by measuring the differences in distance from the tag to all the base stations as Fig. 1(b) shows. The tag broadcasts only one message to every base station for location measuring. Fig. 2(b) shows the time scheme of TDoA. The measured distance difference $\hat{D}_{b_2b_1,t}$ can be calculated as:

$$\hat{D}_{b_2b_1,t} = \hat{D}_{b_2,t} - \hat{D}_{b_1,t} = c\left(T_{b_2,1} - T_{b_1,1}\right) \tag{4}$$

where, $\hat{D}_{b_2,t}$ presents the distance between base station b_2 and tag t, $\hat{D}_{b_1,t}$ denotes the distance between base station b_1 and tag t. The position of tag can be solved by CHAN algorithm [30]:

$$\frac{1}{2}\begin{bmatrix} \hat{D}_{b_2b_1,t} - K_{b_2} + K_{b_1} \\ \hat{D}_{b_3b_1,t} - K_{b_3} + K_{b_1} \\ \vdots \\ \hat{D}_{b_Nb_1,t} - K_{b_N} + K_{b_1} \end{bmatrix}$$

$$= \begin{bmatrix} x_{b_1} - x_{b_2} & y_{b_1} - y_{b_2} & z_{b_1} - z_{b_2} & -\hat{D}_{b_2b_1,t} \\ x_{b_1} - x_{b_3} & y_{b_1} - y_{b_3} & z_{b_1} - z_{b_3} & -\hat{D}_{b_3b_1,t} \\ \vdots & \vdots & \vdots & \vdots \\ x_{b_1} - x_{b_N} & y_{b_1} - y_{b_N} & z_{b_1} - z_{b_N} & -\hat{D}_{b_Nb_1,t} \end{bmatrix} \begin{bmatrix} x_t \\ y_t \\ z_t \\ D_{b_1,t} \end{bmatrix} \tag{5}$$

where:

$$K_S = \|X_S\|^2 \tag{6}$$

The problem can be solved by first assuming that there is no relationship between x_t, y_t, z_t, and $D_{b_1,t}$, and then, solving them by least-square or maximum-likelihood approaches.

One significant benefit of using the TDoA-based system is that it only requires a single message to determine the location of the tag. This allows for a higher update rate and better scalability. Consequently, it is frequently utilized in time-aware scenarios such as unmanned aerial vehicles [31], [32], automatic guided vehicles [33], and real-time locating systems [34], [35]. Tiemann et al. [36] proposed ATLAS, an open-source TDoA-based localization system; This system is designed to be highly scalable, supporting more than 1000 nodes and offering different update rates over 2000Hz.

C. AoA

AoA relies on the angles at which base stations receive the tag's signal to determine the position. As Fig. 1(c) shows, AoA-based base stations are normally equipped with multiple antennas to calculate the angle. Fig. 2(c) shows the time scheme of AoA.

The AoA could be solved through two methods. The first method is to calculate the angle by the difference between each antenna's signal reception time. Suppose the distance between two antennas is d. The AoA can be calculated by:

$$\hat{\theta}_{b_1} = \sin^{-1}\left[\frac{c\left(T_{b_{1a_2},1} - T_{b_{1a_1},1}\right)}{d}\right] \tag{7}$$

The other method is to utilize the phase difference φ_{b_1} to solve AoA:

$$\hat{\theta}_{b_1} = \sin^{-1}\left(\frac{\lambda\varphi}{2\pi d}\right) \tag{8}$$

where λ is the wavelength of UWB signal. After attaining the $\hat{\theta}_{b_1}$ for all base stations, we could solve the position of tag by:

$$X_t = \underset{X_t}{\operatorname{argmin}} \sum_{i=1}^{N} \left(\theta_{b_i} - \hat{\theta}_{b_i}\right)^2 \tag{9}$$

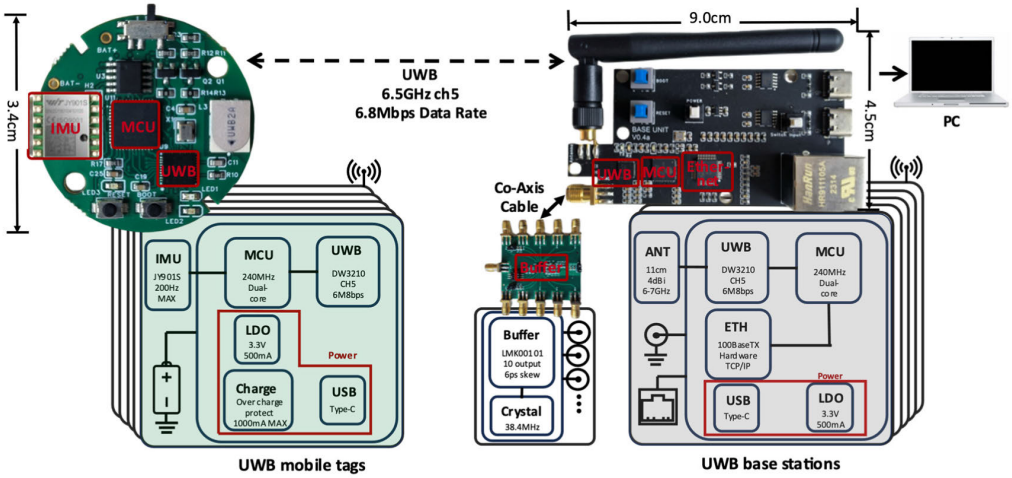

Fig. 3. The proposed UI-MoCap system's architecture diagram describing UWB mobile tags and base stations. Mobile tags are connected wirelessly to UWB network. Base stations are connected to a computer through Ethernet.

where,

$$\theta_{b_i} = \cos^{-1}\left(\frac{\overrightarrow{N}_{b_i}\overrightarrow{b_i t}}{\left|\overrightarrow{b_i t}\right|}\right) \tag{10}$$

$\overrightarrow{N}_{b_i}$ refers to the unit normal vector of the antenna array of base station b_i. $\overrightarrow{b_i t}$ is the vector from base station b_i point to tag t.

The advantage of AoA is that only one message needs to be transmitted to locate the tag, and there is no need to synchronize the base stations. ULoc, proposed by Zhao et al. [37], is a 3D-AoA system that supports azimuth and polar angle measurement simultaneously; The base stations have an L-shaped antenna array containing eight antennas, allowing for the output of the 3D location of tags with centimeter-lever accuracy. However, as an angle-based method, the accuracy of the position is significantly affected by the range. For short-range positions, like chess game positioning [38], AoA provides exceptional accuracy with a median accuracy of 2.4cm. As the positioning range extends, the error proportionally increases. Therefore, for the application of MoCap, the AoA-based system has limited positioning accuracy.

D. Concurrent Technique

Concurrent systems acquire information by listening to signals broadcasted from base stations using full passive tags. Fig. 1(d) shows a kind of concurrent system. Base stations send messages in sequence to the tag for time difference measuring. As Fig. 2(d) shows, the concurrent TDoA time scheme involves tags receiving signals from multiple base stations without having to transmit any signals themselves. This greatly increases scalability, as additional passive tags can be easily added to the system [39], [40], [41], [42], [43], [44]. There are concurrent systems in conjunction with other UWB positioning methods, including Concurrent TWR [42], Concurrent TDoA [40], and Concurrent AoA [41]. Yang et al. proposed the VULoc [42], a virtual-two way ranging (V-TWR) based positioning system; It supports an unlimited number of passive tags and tests for a 7200m^2 large area and reports a 10.5cm median error on location. However, being a receive-only system, the mobile tags do not have the capability to transmit data.

III. System Design and Implementation

In this section, we will introduce the hardware and firmware design of our proposed UI-MoCap system. Fig. 3 provides a presentation of our hardware setup, including the UWB mobile tags and base stations design. All data received from multiple tags are processed by the base stations and transmitted to a computer via a switch. Additionally, we will detail on the system's communication scheme and software platform for 3D positioning and IMU data transmission.

A. UWB Mobile Tag Design

As illustrated in Fig. 3, our UWB wearable tags are primarily composed of three main components: a UWB transceiver, a microcontroller unit (MCU), and an IMU module. The UWB transceiver utilizes the DW3210 chip, with a high-precision oscillator serving as the clock reference. Our choice for the MCU module is the ESP32, which communicates with the DW3210 through a 36MHz SPI interface. To facilitate versatility, we've included a four-pin connector on the PCB, providing 3.3V power support and two configurable communication wires, allowing for the connection of various sensor modules to the tag. For the IMU module, we've opted for the JY901S, which contains a three-axis accelerometer, a three-axis gyroscope, and a three-axis magnetometer. To power the UWB wearable tag, we've integrated a 300mAh Li-ion Battery.

The firmware of our UWB tag is built upon the open-source real-time operating system Zephyr OS. While Zephyr OS provides valuable support for IEEE802.15.4 MAC, we have further customized it to suit our system's specific requirements. This customization includes the development of a driver for the DW3210 chip and modifications to the MAC layer.

There are two primary enhancements we've made to the firmware. Firstly, we've implemented an extended guaranteed time slot (GTS) mechanism, which has expanded the maximum tag count per single superframe from 7 to 255.

Secondly, we've introduced our frame specification to regulate communication between the tags and base stations, which is detailed in Section III-D. The firmware functionality enables the reception of the beacon, decoding of the beacon, and sending data or link requests to base stations.

To ensure the mobility and safety of our wearable tag, it is constructed on a six-layer circular PCB. The board boasts a compact 3.4cm diameter and features strategically placed slots and holes to facilitate easy installation on various devices.

B. UWB Base Station Design

To enable UWB signal reception and precise tag location, we've designed dedicated UWB base stations, as presented in Fig. 3. These UWB base stations consist of three key components including a UWB transceiver, a MCU, and an Ethernet controller.

In line with the UWB tags, we employ the same type of UWB transceiver chips within the base stations. They receive an external clock via a Subminiature Version A (SMA) connector, ensuring precise synchronization with other base stations. The MCU utilized in the base stations shares the same hardware configuration and connections as those in the UWB tags. For Ethernet communication, we've incorporated the W5500 chip to efficiently transmit received IMU data to a computer.

Ensuring synchronized operation across all base stations, we've integrated a dedicated clock generator module. This module is responsible for generating and distributing clock signals to all base stations, ensuring reliable location results. It features a one-to-ten clock buffer and is meticulously manufactured on an impedance-controlled four-layer PCB to maintain the quality of the clock signal.

In terms of firmware, the base stations also rely on the Zephyr OS foundation, with our customized MAC layer. Our system comprises a primary base station, serving as the coordinator, and several sub-base stations that function as passive UWB receivers.

C. Communication Scheme of the System

As depicted in Fig. 4, our communication scheme is divided into two distinct phases, the link phase and the work phase. During the link phase, the computer's address (IP) and open port are transmitted to the base stations for subsequent data transmission. The base station initiates the UWB network, determines the network ID and coordinator address, and starts sending out blank beacons. Powered tags within proximity listen for these beacons, searching for available UWB networks. When a tag captures a beacon, it proactively sends a link request, employing the carrier sense multiple access with collision avoidance (CSMA/CA) protocol. The base station would assign a short address to the tag, and then the tag successfully connects to the UWB network. The base station transmits tag information to the computer, including the tag's address and tag ID. Users can manually set tag configurations on the computer, encompassing adjustable parameters such as frame length, sample rate, active tags, and the sequence of tags. The configuration is then sent to the base stations, completing the link phase of the communication scheme.

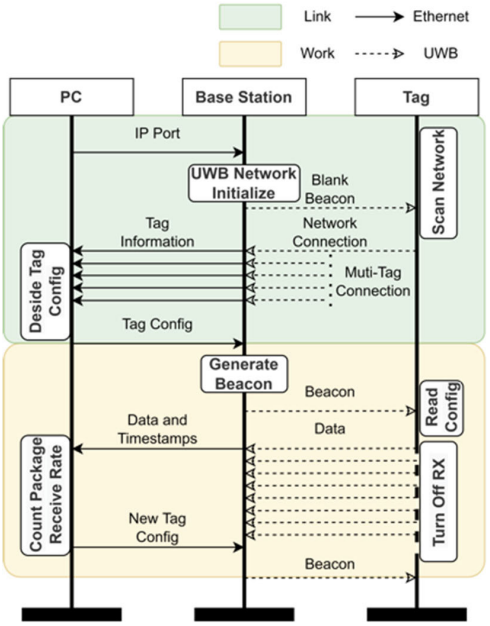

Fig. 4. Communication Scheme of the system. It can be divided into two different phases. Link phase is designed for system initialization and tag connection, and work phase is for IMU data transferring. The arrows present the direction of information flowing.

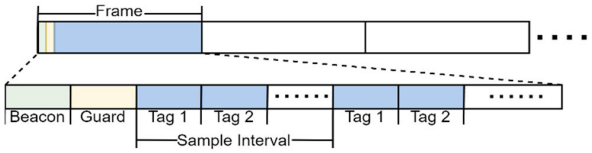

Fig. 5. Time schedule of the work phase. The work phase consists of one-by-one frames. Each frame contains multiple time slots for IMU data transmission.

In the work phase, base stations start to proceed to generate beacons. To prevent the signal collision between tags, the beacon will be sent once every frame time length. When mobile tags receive the beacons, they switch from the receiving state to the transmitting state and start transmitting IMU data to the base station. The base station will send the UWB datasets to the computer through Ethernet.

To manage the IMU data received from multiple tags, each frame within the work phase comprises a sequence of three kinds of slots, including beacon, guard, and tag slots, as depicted in Fig. 5. Firstly, the beacon slot is dedicated to beacon reception. Typically, the length of the beacon signal does not exceed 500 microseconds. However, as the number of scheduled tags increases, the beacon length can exceed 500 microseconds. To account for such situations, we have introduced a guard slot which not only accommodates scenarios where the beacon is larger than 500 microseconds but also prevents signal collisions by allowing sufficient time for tags to switch between transmit and receive states. The third slot arranges the transmitted IMU data from tags according to the sequence of tags. The maximum number of available tags, denoted as N_t, is determined by the sample rate f_s and slot length t_s, which is calculated as follows:

$$N_t < \frac{1}{f_s t_s}. \tag{11}$$

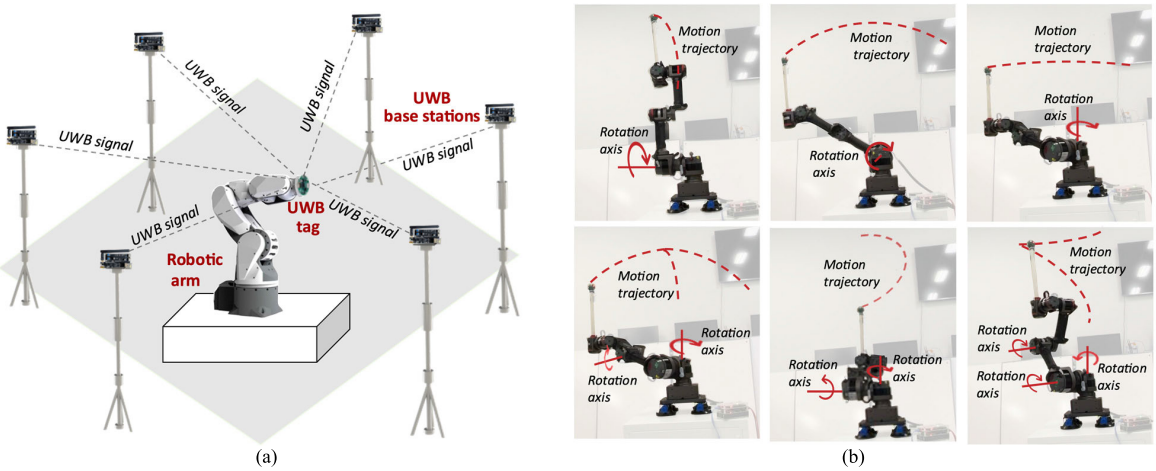

Fig. 6. (a) A schematic diagram of the experimental scenario to evaluate systems' 3D positioning validity and reliability. Several UWB base stations are deployed in the lab environment. A UWB tag is placed at the terminal end of a robotic arm. Reproducible and consistent poses and 3D trajectories can be achieved by manipulating the robotic arm. (b) Six different trajectories involved in the dynamic positioning experiments.

D. Software Platform for Positioning and IMU Data Collection

The computer received UWB datasets from base stations through Ethernet. We have developed an online platform for decoding IMU data and solving position via Python. Our software performs several key functions including UWB data merge, IMU and timestamps extraction and upload, and TDoA positioning calculation to ensure data accuracy and efficient processing.

Firstly, multiple UWB datasets are merged into one data stream. Specifically, UWB data received from multiple base stations are combined, denoted as $\boldsymbol{D} \in \mathbb{R}^{N\times T}$, where N represents the number of base stations and T represents the number of time samples. Then, the integrated UWB data stream $\boldsymbol{D}$ is subjected to a hard-voting machine to determine the majority among N base stations at time t and outputs a final UWB data stream $\boldsymbol{U} \in \mathbb{R}^{1\times T}$. Any incorrect or inconsistent data is filtered out at this stage.

Then, the IMU data and timestamps are decoded from the UWB data stream $\boldsymbol{U} \in \mathbb{R}^{1\times T}$. Firstly, the UWB data stream containing the IMU data and timestamps is converted into a sequence of floating-point numbers. IMU data encompasses motion information of acceleration, angular velocity, magnetic field measurements, and Euler angles. The raw IMU data and the associated timestamps are further uploaded to a cloud server, using the User Datagram Protocol (UDP).

Before calculating the position, a calibration step is required to determine the time deviation of each base station. We utilized the TDoA technique to calculate the tag position. The extracted timestamps are used for calculating tag positions through the CHAN algorithm, detailed in Section II-B. Then, the position performance can be further improved by smoothing with the Kalman filter. The computer also counts the packages and computes the packet receive rate.

IV. Experiments and Data Analysis

A. Experimental Protocols and Data Collection

The first experiment protocol aimed to assess the validity and reliability of 3D positioning in both static and dynamic scenarios. To ensure the execution of reproducible poses and trajectories, we employed a commercial robotic arm (GLUON-6L3, MinTASCA, China), as presented in Fig. 6(a). This robotic arm boasts multiple degrees of freedom (DOFs), enabling to perform predefined trajectories within the bounds of its 3D workspace. To maintain LOS conditions during movement, a 30 cm-long 3D-printed rod was mounted at the terminal end of the robotic arm. A UWB tag was placed at the end of the rod, and seven base stations were positioned in the lab environment to facilitate accurate 3D positioning. Simulations were systematically performed to assess the influence of the number of base stations on positioning accuracy, as detailed in Section I of the Supplementary Document.

The experiments were carried out in a test-retest scenario, comprising static positioning and dynamic positioning tasks conducted over two consecutive days, as two sessions. The system was initially calibrated, a static process lasting one second, before the commencement of experiments. The two session experiments were performed at intervals of more than 24 hours, maintaining the location of the seven UWB base stations. The 24-hour interval was considered appropriate to assess the system's operational reliability.

The static positioning experiment involved five distinct spatial locations. Within each session, the UWB mobile tag was intentionally stationed at different pre-determined locations through precise manipulation of the robotic arm's motion. This stationary stance enabled the collection of positioning data over five seconds. For each static location, the poisoning procedure was repeated five times.

Then, the dynamic positioning analysis involved six diverse spatial motion trajectories, as illustrated in Fig. 6(b). The UWB mobile tag performed a round-trip along each pre-determined trajectory under controlled robotic arm motions. The robotic arm maintained a consistent velocity magnitude ranging from 0.1 to 0.3 m/s, depending on the specific trajectory, while acceleration and deceleration phases were executed at approximately 10 m/s^2 for acceleration. Our system recorded the tag's positioning data throughout the entire dynamic trajectories. The rigorous protocol required the repetition of this process five times for each trajectory.

To evaluate the positioning accuracy of the proposed system, we attached an optical reflection maker to the UWB mobile tag, and accurately recorded the position of the UWB mobile tag through the optical MoCap system (Raptor-4S, Motion Analysis Corporation, USA), which was the gold standard for evaluation.

The second experimental protocol was designed to evaluate the packet loss rates of IMU data transmission from multiple UWB tags. The experiments involved simultaneous IMU data transmission from 10 designed UWB tags as transmitters to a base station serving as the receiver.

Firstly, to explore the anti-signal interference ability of the system, we compared the packet loss rate between UWB and Wi-Fi both at in-lab and out-lab environments. For comparison, we also applied 10 commercial IMUs of the same type (JY901, Wit-motion, China) via Wi-Fi. The transmitters and receiver were placed at a distance of 2m, and signal transmission continued for 30min at a transmission frequency of 100Hz. The in-lab environment was a typical electrical engineering lab setting with strong interference effects. More than 60 devices, including smartphones, laptop, and other electronic equipment, were simultaneously in operation. The out-lab environment was a spacious corridor that was devoid of electronic devices, resulting in significantly lower signal interference.

Furthermore, we investigated the packet loss rate of IMU data transmission at different transmission distances. In this scenario, 10 designed UWB tags simultaneously transmitted IMU signals. The transmission distances were set at 2m, 7m, 12m, 17m and 22m, with each distance maintaining continuous data transmission for 30min at an update rate of 100Hz.

B. Data Analysis

The efficacy of the proposed UI-MoCap system is subjected to a comprehensive assessment, spanning both system validity and reliability. Additionally, an examination of packet loss is undertaken, further enriched through a systematic comparison with Wi-Fi-based alternatives.

The collected location data undergoes initial post-processing via down-sampling using a mean filter. This filter, defined by a kernel size of four and a step length of four, reduces the data frequency from 100 Hz to 25 Hz. This step was applied after Kalman filtering, ensuring a minimal impact on positioning accuracy while decreasing the data samples.

1) Positioning Accuracy Measurements: The positioning validity of the proposed system is assessed through an analysis of positioning errors. In the context of 3D spatial positioning, the evaluation entails the computation of absolute errors (AEs) across distinct domains: $AE_{(x,y)}$ for the (x, y) 2D domain, AE_{Z-axis} for the vertical Z-axis, and AE_{3D} for the complete (x, y, z) 3D domain. These metrics are mathematically formulated as follows:

$$AE_{(x,y)} = \frac{\Sigma_{n=1}^{N}\sqrt{(x_n-\hat{x}_n)^2+(y_n-\hat{y}_n)^2}}{N} \tag{12}$$

$$AE_{Z-axis} = \frac{\Sigma_{n=1}^{N}\sqrt{(z_n-\hat{z}_n)^2}}{N} \tag{13}$$

$$AE_{3D} = \frac{\Sigma_{n=1}^{N}\sqrt{(x_n-\hat{x}_n)^2+(y_n-\hat{y}_n)^2+(z_n-\hat{z}_n)^2}}{N} \tag{14}$$

where the coordinates (x_n, y_n, z_n) correspond to the 3D position as measured by UI-MoCap at the n^{th} time sample. $(\hat{x}_n, \hat{y}_n, \hat{z}_n)$ present the 3D position captured by the optical MoCap system at the same time sample. The variable N denotes the total counts of time samples involved in the analysis.

2) Intra-Session and Inter-Session Correlation Coefficients: The proposed system's reliability is assessed through an analysis of the Pearson correlation coefficient (CC), which evaluates the similarity between measured trajectories across trials. CC is formulated as follows:

$$CC = \frac{\sum_n (x_n-\bar{x})\cdot(y_n-\bar{y})\cdot(z_n-\bar{z})}{\sqrt{\sum_n (x_i-\bar{x})^2\cdot\sum_n (y_i-\bar{y})^2\cdot\sum_n (z_n-\bar{z})^2}} \tag{15}$$

where the coordinates (x_n, y_n, z_n) correspond to the 3D position as measured by UI-MoCap at the n^{th} time sample. $\bar{x}$, $\bar{y}$, and $\bar{z}$ present the average value of x_n, y_n, and z_n, respectively, computed across the recorded samples.

For the test-retest reliability, we have proposed intra-session CC and inter-session CC. The intra-session CC is to evaluate the similarity between measured dynamic trajectories within a single session's trials, while the inter-session CC gauges the comparability of dynamic trajectories across trials conducted in two distinct sessions. Augmenting this analysis, the intra-session and inter-session CC are subjected to a Wilcoxon test, conducted at a 95% confidence level. This statistical validation supplements the correlation analysis, thus contributing to a robust evaluation of the system's reliability in capturing consistent positioning data.

3) Average Packet Loss Rate: The packet loss rate serves as a pivotal metric to discern the system's capability to transmit IMU signals. The average packet loss rate (*APLR*) is quantified through the following calculation:

$$APLR = \frac{1}{T}\cdot\Sigma_{t=1}^{T}\left(\frac{1}{K}\Sigma_{k=1}^{K}\frac{N_{rk}}{N_{tk}}\right) \tag{16}$$

where N_{tk} denotes the number of samples transmitted by the k^{th} IMU transmitter (i.e., UWB tags or IMU), while N_{rk} corresponds to the number of samples successfully received by the computer; K presents the total number of IMU transmitters, and T denotes the total duration of packet transmission.

V. Experimental Results and Discussion

The effectiveness of the proposed UI-MoCap system is thoroughly evaluated through a series of experiments. The outcomes of 3D positioning errors both in static and dynamic scenarios are vividly depicted in Fig. 7, 8, and 9. Secondly, an exploration of the system's reliability is presented in the findings of Fig. 10. Furthermore, the packet loss rate of IMU data transmission from multiple tags is shown in Fig. 11.

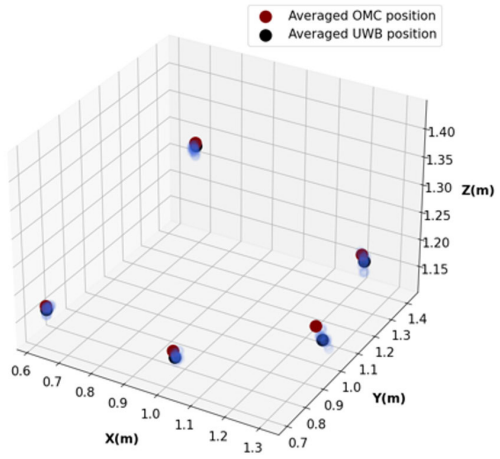

Fig. 7. The positioning performance in static experiments. The blue shading denotes the collection of measured positions at time samples in trials. The black dot represents the average position among trials recorded by UI-MoCap, and the red dot corresponds to the average position recorded by the optical MoCap system (OMC).

A. System Validity

Firstly, we evaluate the positioning accuracy of UI-MoCap in static scenarios. The UWB mobile tag is securely affixed to the robotic arm's extremity and positioned at five distinct locations. The corresponding positioning outcomes are presented in Fig. 7. The blue shading denotes the collection of measured positions at time samples in trials. The black dot represents the average position among trials recorded by UI-MoCap, and the red dot corresponds to the average position recorded by the optical MoCap system.

Secondly, we further evaluate the system's tracking accuracy during dynamic operations. Similarly, the UWB mobile tag remains affixed to the robotic arm's extremity and undergoes six distinct dynamic trajectories, as presented in Fig. 6(b). The positioning performance are illustrated in Fig. 8. The blue shading captures the collection of tracking points sampled from all trials. The black line traces the trajectory average from among these trials, while the red line represents the average trajectory among trials recorded by the optical MoCap system.

The averaged *AE* in both static and dynamic positioning is shown in Fig. 9(a). Additionally, Fig. 9(b) shows the cumulative probability distribution of 3D positioning *AE*. In the context of static scenario, the averaged position *AE* is 1.03cm, 1.41cm, 1.86cm within 2D, Z-axis, and 3D domains, respectively. Furthermore, the system achieves 3D positioning *AE*s of {1.34, 3.37, 4.19cm} at {50^{th}, 90^{th}, 95^{th}}, respectively. Within dynamic scenario, the averaged positioning *AE* is 1.76cm, 2.13cm, 3.20cm in 2D, Z-axis domain, and 3D domains, respectively. It achieves 3D positioning *AEs* of merely {2.20, 5.15, 6.39}cm at {50^{th}, 90^{th}, 95^{th}} percentile, respectively.

B. System Reliability

In order to assess the reliability of our proposed system, we conducted the test-retest experiments and performed an analysis encompassing both intra-session and inter-session correlations. These results are visually depicted in Fig. 10. The intra-session CC is lager in magnitude compared to inter-session CC. It is noteworthy that both the intra-session and inter-session CCs surpass the significant threshold of 0.990, which is analyzed with the Wilcoxon test ($p < 0.0001$). This outcome serves to underscore the remarkably high level of reliability inherent to our system. The substantial CCs in both intra-session and inter-session contexts affirm that our system reliably maintains its performance across various testing scenarios.

C. APLR of IMU Data Transmission From Multiple Tags

The *APLR* of UI-MoCap is depicted when employing 10 designed UWB tags for IMU data transmission, and it is compared with 10 commercial IMUs of the same type, transmitting IMU data via Wi-Fi, both at in-lab and out-lab environment. In Fig. 11(a), in both settings, the *APLR* of UI-MoCap is significantly lower than that of Wi-Fi. The average values with standard deviation of packet loss rates for our system are $0.032 \pm 0.034\%$ and $0.041 \pm 0.035\%$ at in-lab and out-lab environments, respectively. However, for Wi-Fi, the average with standard deviation of packet loss rates is $2.004 \pm 7.536\%$ and $0.168 \pm 0.937\%$ in at in-lab and out-lab environments, respectively. Notably, at the in-lab environment, Wi-Fi experiences a significant increase in *APLR*, and the standard deviation exceeds three times the average, indicating unstable IMU data transmission over time. This instability is attributed to signal interference. Conversely, The *APLR* of UI-MoCap based on UWB technology remains nearly unaffected, underscoring UWB's substantial advantage in maintaining robust IMU data transmission compared to Wi-Fi.

Fig. 11(b) illustrates the *APLR* of multiple UWB tags for different transmission distances. Ten UWB tags are placed at the distance of 2m, 7m, 12m, 17m, and 22m from the UWB base station for IMU data transmission, resulting in *APLRs* of 0.041%, 0.040%, 0.143%, 88.575% and 96.714%, respectively. A significant increase in *APLR* is observed at distances ranging from 12m to 22m. This increase suggests that UWB tags positioned larger than this range struggle to receive beacon frames from the UWB base stations.

D. Results and Discussion

To the best of our knowledge, this work marks the first instance of fusing multiple IMU data transmission with UWB positioning technology at the hardware level, resulting in both high-accuracy 3D positioning and a high update rate for IMU data transmission. Our findings demonstrate that the system achieves remarkable 3D positioning accuracy in LOS scenarios, with a positioning error of 1.86cm in static experiments and 3.20cm in dynamic tests. The system also exhibits excellent robustness in test-retest scenarios. Additionally, in the same environmental conditions, our system's IMU data transmission exhibits a significantly lower packet loss rate compared to IMU data transmission via Wi-Fi at 100 Hz update rate. Hence, our UI-MoCap system can be considered valid and reliable.

Among the typical deployment methods introduced in Section. II for UWB positioning systems, the TDoA-based positioning approach emerges as the most suitable choice, as it enables reliable IMU data transmission while maintaining high-precision 3D positioning. While TWR-based

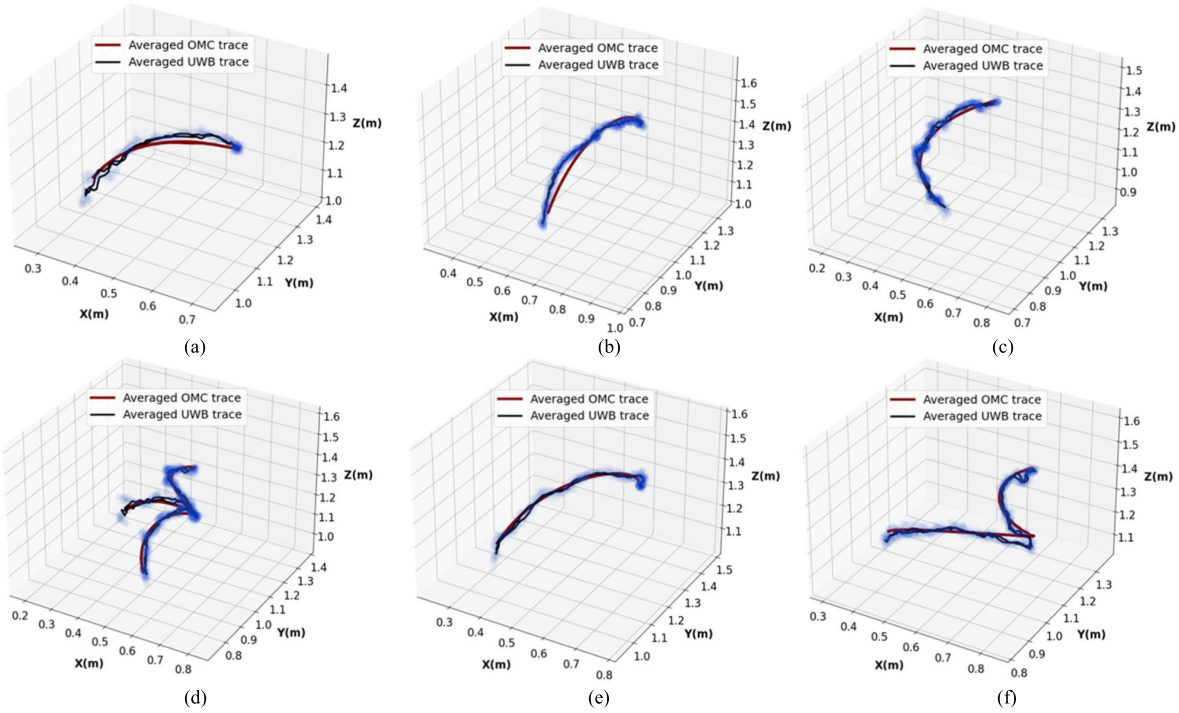

Fig. 8. The positioning performance in dynamic experiments. (a)-(f) Results of six distinct dynamic trajectories performed by a robotic arm. The blue shading captures the collection of tracking points sampled from all trials. The black line traces the trajectory average among these trials, while the red line represents the average trajectory among trials recorded by the optical MoCap system (OMC).

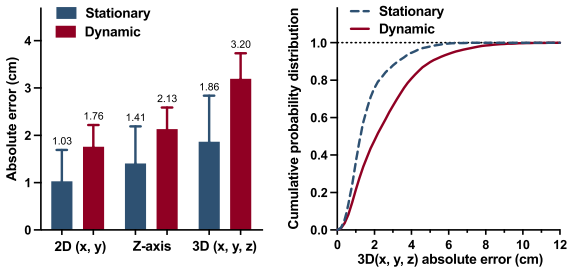

Fig. 9. (a) The averaged absolute error within 2D, Z-axis, and 3D domains in both static and dynamic positioning experiments. (b) The cumulative probability distribution of absolute error in 3D domain.

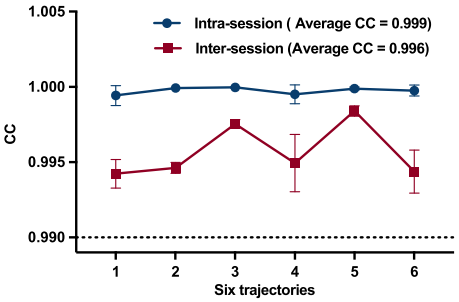

Fig. 10. The intra-session and inter-session correlation coefficients (CC) for test-retest reliability. The significant threshold is 0.990 at a 95% confidence level ($p < 0.0001$).

methods offer exceptional positioning accuracy, they involve the exchange of numerous messages to determine a tag's location, resulting in redundant communication. For instance, Kempke et al. [45] introduced a TWR-based positioning system named SurePoint, which necessitated the transmission of 30 packages to determine a tag's location when using three base stations. Such intricate data transmission processes lead

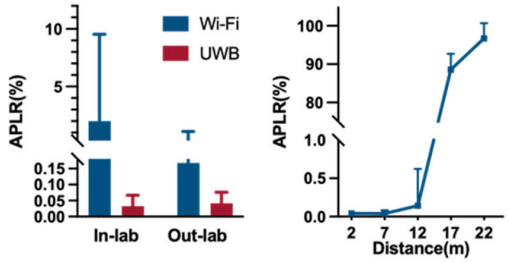

Fig. 11. (a) The average packet loss rate (APLR) of proposed system and Wi-Fi both at in-lab and out-lab environments. (b) The APLR of multiple UWB tags for different transmission distances.

to lower update rates, rendering it unsuitable for scenarios involving moving objects due to latency and IMU signal transmission. For AoA-based positing systems, they could offer advantages of high update rates and cost-effective deployment. However, their positioning accuracy is significantly affected by the positioning range. For example, if an AoA-based system has 2cm error within 1m positioning range, this error would be amplified to 20cm when extending the positioning distance to 10m. On the other hand, concurrent-based positioning is a receive-only system incapable of transmitting IMU data to a computer. TDoA-based methods are preferable due to their high update rates, low latency, modest power consumption for packet transmission, and superior location accuracy when base stations are well-synchronized. For instance, Tiemann et al. [36] proposed ATLAS, an open-source TDoA-based localization system capable of supporting over 1000 nodes with various update rates concurrently. Therefore, the TDoA-based method is the most suitable choice for system deployment that satisfies both IMU signal transmission and reliable 3D positioning.

TABLE I
EXISTING AND THE PROPOSED UWB-BASED POSITIONING SYSTEMS

Ref.	System	Technique	Positioning Accuracy (cm)		Dimension	Update Rate	Multiple Tags
			Static	Dynamic			
[37]	ULoc	3D AoA	3.6	8	3D	Not report	9
[40]	SnapLoc	Concurrent TDoA	17	/	2D	996Hz	Un-limited
[41]	AnguLoc	Concurrent AoA	30	/	2D	Not report	8
[42]	VULoc	V-TWR	10.5	11.7	2D	Not report	Un-limited
[43]	FlexTDOA	Concurrent TDoA	10.6	/	3D	Not report	Un-limited
[45]	SurePoint	ToF	29	/	3D	1-12Hz	12
[46]	Chiasson *et al.*	AltDS-TWR	11.6	/	3D	Not report	Un-limited
	UI-MoCap	TDoA	**1.86**	**3.20**	3D	100-1000Hz	10

Table I provides an overview of recent indoor UWB positioning technologies focusing on LOS scenarios, highlighting our system's competitive positioning accuracy. The improvement in positioning accuracy is attributed to three main factors. Firstly, our system employs a wired synchronization strategy using a centralized clock generator connected to base stations via cables, minimizing skew compared to the wireless synchronization used by other studies listed in Table I. Secondly, our system applied the newer DW3210 UWB transceiver chip, offering a precision of ± 6cm [47], while UWB systems in Table I predominantly use the DW1000 chip with ±10 cm precision [48]. This hardware upgrade contributes to enhanced precision. Lastly, the integration of a Kalman filter in our software effectively mitigates UWB noise, further improving positioning accuracy. The impact of the Kalman filter on positioning accuracy in stationary and dynamic tests was demonstrated in the Section. II of Supplementary Document. Some studies in Table I also applied processing methods to achieve better position performance, including Kalman filter [37], extended Kalman filter [40], and median filter [45]. In addition, the optimized MAC layer design in our proposed UWB wearable tag enhances the overall system's update rate and power efficiency by reducing scheduling payload. Detailed power consumption analysis was provided in the Supplementary Document.

Our system is targeted toward indoor MoCap applications in gaming, sports, rehabilitation, human-robot interactions, etc., where involves unavoidable magnetic disturbance from electrical equipment. In contrary to IMU-based wearable MoCap systems that are drift-prone over time, our system could provide absolute 3D position of multiple wearable tags while ensuring robust IMU data transmission and recording. To enhance its capabilities further, our system could be further developed by integrating extended Kalman filtering, fusing the UWB positioning and IMU signals, to guarantee a robust and continuous 3D positioning of full-body motion in both LOS and NLOS conditions.

Our study still has some limitations. First of all, although UI-MoCap has the capability for multi-tag positioning, we have conducted 3D positioning experiments using only one tag; Although this does not affect our assessment of the system's effectiveness, future work should consider including multi-tag positioning accuracy tests to broaden the scope of experimentation. Secondly, UI-MoCap has achieved high 3D positioning accuracy and reliable IMU data transmission; However, there is a need for the development of algorithms that can effectively integrate UWB positioning and IMU data, further enhancing positioning accuracy. Thirdly, the hardware design was suboptimized for power consumption. A better parts selection in next generation would improve the operation duration of the system.

VI. CONCLUSION

This research presents a pioneering effort in building up a UI-MoCap system that seamlessly integrates multiple IMU data transmission with UWB positioning technology at the hardware level. The UWB mobile tags, equipped with IMU modules, transmit IMU data though UWB to base stations. The hardware-synchronized base stations effectively manage IMU data transmission from multiple tags. The system's validity and reliability have been tested in both static and dynamic scenarios, revealing several key findings: 1) centimeter-level 3D positioning accuracy, with a positioning error of 1.86cm in static experiments and 3.20cm in dynamic tests, 2) robust positioning performance over time, as demonstrated by a test-retest study, and 3) a high update rate and low packet loss rate for IMU data transmission, surpassing the efficiency of Wi-Fi-based transmission techniques. The proposed system holds significant potential for enhancing sensor fusion techniques involving IMU and UWB signals, thereby improving positioning accuracy and long-term robustness for MoCap applications.

REFERENCES

[1] C. M. N. Brigante, N. Abbate, A. Basile, A. C. Faulisi, and S. Sessa, "Towards miniaturization of a MEMS-based wearable motion capture system," *IEEE Trans. Ind. Electron.*, vol. 58, no. 8, pp. 3234–3241, Aug. 2011.

[2] A. M. Aurand, J. S. Dufour, and W. S. Marras, "Accuracy map of an optical motion capture system with 42 or 21 cameras in a large measurement volume," *J. Biomechanics*, vol. 58, pp. 237–240, Jun. 2017.

[3] E. van der Kruk and M. M. Reijne, "Accuracy of human motion capture systems for sport applications; state-of-the-art review," *Eur. J. Sport Sci.*, vol. 18, no. 6, pp. 806–819, Jul. 2018.

[4] C. Bregler, "Motion capture technology for entertainment [in the spotlight]," *IEEE Signal Process. Mag.*, vol. 24, no. 6, pp. 158–160, Nov. 2007.

[5] D. Vogt, S. Stepputtis, S. Grehl, B. Jung, and H. Ben Amor, "A system for learning continuous human-robot interactions from human-human demonstrations," in *Proc. IEEE Int. Conf. Robot. Autom. (ICRA)*, May 2017, pp. 2882–2889.

[6] X. Fu et al., "Gait cycle-inspired learning strategy for continuous prediction of knee joint trajectory from sEMG," 2023, *arXiv:2307.13209*.

[7] C. D. Metcalf et al., "Markerless motion capture and measurement of hand kinematics: Validation and application to home-based upper limb rehabilitation," *IEEE Trans. Biomed. Eng.*, vol. 60, no. 8, pp. 2184–2192, Aug. 2013.

[8] H. Liu et al., "Close-range human following control on a cane-type robot with multi-camera fusion," *IEEE Robot. Autom. Lett.*, vol. 8, no. 10, pp. 6443–6450, Oct. 2023.

[9] M. N. H. Yunus, M. H. Jaafar, A. S. A. Mohamed, N. Z. Azraai, and M. S. Hossain, "Implementation of kinetic and kinematic variables in ergonomic risk assessment using motion capture simulation: A review," *Int. J. Environ. Res. Public Health*, vol. 18, no. 16, p. 8342, Aug. 2021.

[10] M. El-Gohary and J. McNames, "Shoulder and elbow joint angle tracking with inertial sensors," *IEEE Trans. Biomed. Eng.*, vol. 59, no. 9, pp. 2635–2641, Sep. 2012.

[11] L. Atallah, B. Lo, R. King, and G.-Z. Yang, "Sensor positioning for activity recognition using wearable accelerometers," *IEEE Trans. Biomed. Circuits Syst.*, vol. 5, no. 4, pp. 320–329, Aug. 2011.

[12] D. Feng, C. Wang, C. He, Y. Zhuang, and X.-G. Xia, "Kalman-filter-based integration of IMU and UWB for high-accuracy indoor positioning and navigation," *IEEE Internet Things J.*, vol. 7, no. 4, pp. 3133–3146, Apr. 2020.

[13] E. Foxlin, "Pedestrian tracking with shoe-mounted inertial sensors," *IEEE Comput Graph Appl.*, vol. 25, no. 6, pp. 38–46, Dec. 2005.

[14] Q. Yuan and I. Chen, "3-D localization of human based on an inertial capture system," *IEEE Trans. Robot.*, vol. 29, no. 3, pp. 806–812, Jun. 2013.

[15] B. Gulmezoglu, M. B. Guldogan, and S. Gezici, "Multiperson tracking with a network of ultrawideband radar sensors based on Gaussian mixture PHD filters," *IEEE Sensors J.*, vol. 15, no. 4, pp. 2227–2237, Apr. 2015.

[16] R. Bharadwaj, S. Swaisaenyakorn, C. G. Parini, J. Batchelor, and A. Alomainy, "Localization of wearable ultrawideband antennas for motion capture applications," *IEEE Antennas Wireless Propag. Lett.*, vol. 13, pp. 507–510, 2014.

[17] M. Di Renzo, R. M. Buehrer, and J. Torres, "Pulse shape distortion and ranging accuracy in UWB-based body area networks for full-body motion capture and gait analysis," in *Proc. IEEE Glob. Telecommun. Conf.*, Nov. 2007, pp. 3775–3780.

[18] S. Marano, W. Gifford, H. Wymeersch, and M. Win, "NLOS identification and mitigation for localization based on UWB experimental data," *IEEE J. Sel. Areas Commun.*, vol. 28, no. 7, pp. 1026–1035, Sep. 2010.

[19] Y. Gu, A. Lo, and I. Niemegeers, "A survey of indoor positioning systems for wireless personal networks," *IEEE Commun. Surveys Tuts.*, vol. 11, no. 1, pp. 13–32, 1st Quart., 2009.

[20] M. Gunia, F. Protze, N. Joram, and F. Ellinger, "Setting up an ultra-wideband positioning system using off-the-shelf components," in *Proc. 13th Workshop Positioning, Navigat. Commun. (WPNC)*, Oct. 2016, pp. 1–6.

[21] Y. Zhong, T. Liu, B. Li, L. Yang, and L. Lou, "Integration of UWB and IMU for precise and continuous indoor positioning," in *Proc. Ubiquitous Positioning, Indoor Navigat. Location-Based Services (UPINLBS)*, Mar. 2018, pp. 1–5.

[22] S. Zihajehzadeh, P. K. Yoon, B.-S. Kang, and E. J. Park, "UWB-aided inertial motion capture for lower body 3-D dynamic activity and trajectory tracking," *IEEE Trans. Instrum. Meas.*, vol. 64, no. 12, pp. 3577–3587, Dec. 2015.

[23] S. Zihajehzadeh and E. J. Park, "A novel biomechanical model-aided IMU/UWB fusion for magnetometer-free lower body motion capture," *IEEE Trans. Syst. Man, Cybern. Syst.*, vol. 47, no. 6, pp. 927–938, Jun. 2017.

[24] P. K. Yoon, S. Zihajehzadeh, B.-S. Kang, and E. J. Park, "Robust biomechanical model-based 3-D indoor localization and tracking method using UWB and IMU," *IEEE Sensors J.*, vol. 17, no. 4, pp. 1084–1096, Feb. 2017.

[25] M. Ridolfi, S. Van De Velde, H. Steendam, and E. De Poorter, "Analysis of the scalability of UWB indoor localization solutions for high user densities," *Sensors*, vol. 18, no. 6, p. 1875, Jun. 2018.

[26] D. Neirynck, E. Luk, and M. McLaughlin, "An alternative double-sided two-way ranging method," in *Proc. 13th Workshop Positioning, Navigat. Commun. (WPNC)*, Oct. 2016, pp. 1–4.

[27] B. Barua, N. Kandil, and N. Hakem, "On performance study of TWR UWB ranging in underground mine," in *Proc. 6th Int. Conf. Digit. Inf., Netw., Wireless Commun. (DINWC)*, Apr. 2018, pp. 28–31.

[28] F. Bonnin-Pascual and A. Ortiz, "An UWB-based system for localization inside merchant vessels," in *Proc. 24th IEEE Int. Conf. Emerg. Technol. Factory Autom. (ETFA)*, Sep. 2019, pp. 1559–1562.

[29] S. Sung, H. Kim, and J.-I. Jung, "Accurate indoor positioning for UWB-based personal devices using deep learning," *IEEE Access*, vol. 11, pp. 20095–20113, 2023.

[30] Y. T. Chan and K. C. Ho, "A simple and efficient estimator for hyperbolic location," *IEEE Trans. Signal Process.*, vol. 42, no. 8, pp. 1905–1915, Aug. 1994.

[31] J. Tiemann, F. Schweikowski, and C. Wietfeld, "Design of an UWB indoor-positioning system for UAV navigation in GNSS-denied environments," in *Proc. Int. Conf. Indoor Positioning Indoor Navigat. (IPIN)*, Oct. 2015, pp. 1–7.

[32] J. Tiemann and C. Wietfeld, "Scalable and precise multi-UAV indoor navigation using TDOA-based UWB localization," in *Proc. Int. Conf. Indoor Positioning Indoor Navigat. (IPIN)*, Sep. 2017, pp. 1–7.

[33] P. Verde, J. Díez-González, R. Álvarez, and H. Perez, "Characterization of AGV localization system in industrial scenarios using UWB technology," *IEEE Trans. Instrum. Meas.*, vol. 72, pp. 1–13, 2023.

[34] S. Bottigliero, D. Milanesio, M. Saccani, and R. Maggiora, "A low-cost indoor real-time locating system based on TDOA estimation of UWB pulse sequences," *IEEE Trans. Instrum. Meas.*, vol. 70, pp. 1–11, 2021.

[35] F. Zhang, L. Yang, Y. Liu, Y. Ding, S.-H. Yang, and H. Li, "Design and implementation of real-time localization system (RTLS) based on UWB and TDoA algorithm," *Sensors*, vol. 22, no. 12, p. 4353, Jun. 2022.

[36] J. Tiemann, Y. Elmasry, L. Koring, and C. Wietfeld, "ATLAS FaST: Fast and simple scheduled TDOA for reliable ultra-wideband localization," in *Proc. Int. Conf. Robot. Autom. (ICRA)*, May 2019, pp. 2554–2560.

[37] M. Zhao, T. Chang, A. Arun, R. Ayyalasomayajula, C. Zhang, and D. Bharadia, "ULoc: Low-power, scalable and CM-accurate UWB-tag localization and tracking for indoor applications," *Proc. ACM Interact., Mobile, Wearable Ubiquitous Technol.*, vol. 5, no. 3, pp. 1–31, 2021.

[38] A. Arun, S. Saruwatari, S. Shah, and D. Bharadia, "XRLoc: Accurate UWB localization to realize XR deployments," 2023, *arXiv:2307.12512*.

[39] A. Ledergerber, M. Hamer, and R. D'Andrea, "A robot self-localization system using one-way ultra-wideband communication," in *Proc. IEEE/RSJ Int. Conf. Intell. Robots Syst. (IROS)*, Sep. 2015, pp. 3131–3137.

[40] B. Großiwindhager, M. Stocker, M. Rath, C. A. Boano, and K. Römer, "SnapLoc: An ultra-fast UWB-based indoor localization system for an unlimited number of tags," in *Proc. 18th ACM/IEEE Int. Conf. Inf. Process. Sensor Netw. (IPSN)*, Apr. 2019, pp. 61–72.

[41] M. Heydariaan, H. Dabirian, and O. Gnawali, "AnguLoc: Concurrent angle of arrival estimation for indoor localization with UWB radios," in *Proc. 16th Int. Conf. Distrib. Comput. Sensor Syst. (DCOSS)*, May 2020, pp. 112–119.

[42] J. Yang, B. Dong, and J. Wang, "VULoc: Accurate UWB localization for countless targets without synchronization," *Proc. ACM Interact. Mobile Wearable Ubiquitous Technol.*, vol. 6, no. 3, pp. 1–25, 2022.

[43] G.-C. Patru, L. Flueratoru, I. Vasilescu, D. Niculescu, and D. Rosner, "FlexTDOA: Robust and scalable time-difference of arrival localization using ultra-wideband devices," *IEEE Access*, vol. 11, pp. 28610–28627, 2023.

[44] L. Santoro, M. Nardello, D. Brunelli, and D. Fontanelli, "UWB-based indoor positioning system with infinite scalability," *IEEE Trans. Instrum. Meas.*, vol. 72, pp. 1–11, 2023.

[45] B. Kempke, P. Pannuto, B. Campbell, and P. Dutta, "SurePoint: Exploiting ultra wideband flooding and diversity to provide robust, scalable, high-fidelity indoor localization," in *Proc. 14th ACM Conf. Embedded Netw. Sensor Syst. (CD-ROM)*, Nov. 2016, pp. 137–149.

[46] D. Chiasson, Y. Lin, M. Kok, and P. B. Shull, "Asynchronous hyperbolic UWB source-localization and self-localization for indoor tracking and navigation," *IEEE Internet Things J.*, vol. 10, no. 13, pp. 11655–11668, Jul. 2023.

[47] *DW3000 User Manual*, May 2021.

[48] *DW1000 Data Sheet*, Dec. 2017.